

# Calibration of nuclear recoils at the 100 eV scale using neutron capture

L. Thulliez,<sup>1</sup> D. Lhuillier,<sup>1,\*</sup> A. Chebboubi,<sup>2</sup> E. Dumonteil,<sup>1</sup> A. Erhart,<sup>3</sup> A. Giuliani,<sup>4</sup> F. Gunsing,<sup>1</sup> E. Jericha,<sup>5</sup> M. Kaznatcheeva,<sup>3</sup> A. Kinast,<sup>3</sup> A. Langenkämper,<sup>3</sup> T. Lasserre,<sup>1,3</sup> A. Letourneau,<sup>1</sup> O. Litaize,<sup>2</sup> P. de Marcillac,<sup>4</sup> S. Marnieros,<sup>4</sup> T. Materna,<sup>1</sup> B. Mauri,<sup>1</sup> C. Nones,<sup>1</sup> T. Ortmann,<sup>3</sup> L. Pattavina,<sup>3,6</sup> D.V. Poda,<sup>4</sup> R. Rogly,<sup>1</sup> N. Schermer,<sup>3</sup> O. Serot,<sup>2</sup> G. Soum,<sup>1</sup> L. Stodolsky,<sup>7</sup> R. Strauss,<sup>3</sup> M. Vivier,<sup>1</sup> V. Wagner,<sup>3</sup> and A. Wex<sup>3</sup>

<sup>1</sup>*IRFU, CEA, Université Paris-Saclay, 91191 Gif-sur-Yvette, France*

<sup>2</sup>*CEA, DES, IRESNE, DER, Cadarache F-13108 Saint-Paul-Lez-Durance, France*

<sup>3</sup>*Physik-Department, Technische Universität München, D-85748 Garching, Germany*

<sup>4</sup>*Université Paris-Saclay, CNRS/IN2P3, IJCLab, 91405 Orsay, France*

<sup>5</sup>*TU Wien, Atominstytut, 1020 Wien, Austria*

<sup>6</sup>*INFN, Laboratori Nazionali del Gran Sasso, 67100 Assergi, Italy*

<sup>7</sup>*Max-Planck-Institut für Physik, D-80805 München, Germany*

(Dated: April 24, 2022)

The development of low-threshold detectors for neutrinos and dark matter necessitates low-energy calibration. We suggest this can be provided by the nuclear recoils resulting from the  $\gamma$  emission following neutron capture. There is often a well defined MeV-scale  $\gamma$  associated to a nuclear recoil in the 100 eV range. Using the FIFRELIN code,  $\gamma$ -cascades of various isotopes can be predicted with high accuracy. We present a comprehensive experimental concept for the calibration of  $\text{CaWO}_4$  and Ge cryogenic detectors and show the potential of additional  $\gamma$  tagging to extend the reach of the method.

**PACS numbers:**

Major advances in low-threshold detector technology have opened up new avenues for low-mass Dark Matter (DM) searches [1–4] and coherent elastic neutrino-nucleus scattering (CEvNS) [5, 6]. Steeply rising signal rates towards low energies, as expected for light-mass DM or CEvNS at nuclear reactors, entail a high discovery potential for new physics with miniaturized detectors. In recent years, the energy threshold for nuclear recoils has been reduced from the keV regime to several 10's of eV by new-generation macroscopic low-temperature detectors [7–11]. Accessing this new energy range, however, may raise fundamental questions about phonon-mediated detectors and imply uncertainties in the detector response. The lack of calibration sources at sub-keV energies is currently by-passed by simple extrapolation from well-understood keV-scale energies [12, 13] or by relying on model-dependent predictions [14–16]. However, new-generation rare-event searches require accurate calibration of nuclear recoils—the experimental signature of DM and CEvNS experiments—on a percent level. This can also give insights into atomic and solid-state physics at these low energies.

We propose here a new method for calibrating nuclear recoils in the 100 eV range based on the capture of thermal neutrons. The negligible kinetic energy of the captured neutron ( $\approx 25$  meV) puts the compound nucleus at an excited state close to the neutron separation energy  $S_n$ , of several MeV. This state decays via  $\gamma$ -ray and conversion electron emission. Although there is typically a complicated multi- $\gamma$  cascade, there is often a primary transition with a substantial probability, going from the  $S_n$  state directly to the ground state (single- $\gamma$ ). This highest energy photon easily escapes cm-scale detectors

and the resulting nuclear recoil is typically in the 100 eV range for middle and heavy mass nuclei. We emphasize that this neutron probe samples the full volume of 1–100 g detector, whose dimensions are similar to the penetration depth of thermal neutrons. The calibration method is most suited for low-threshold cryogenic detectors operated at mK temperatures [17] – in the following called 'detectors' – but may also be applied to other types of particle detectors in the future.

A suitable target nucleus has a high natural abundance ( $Y_{ab}$ ) and a high thermal n-capture cross-section ( $\sigma_{n,\gamma}$ ). The compound nucleus should have a sizeable branching ratio for the single- $\gamma$  transitions ( $I_\gamma^s$ ), although multi- $\gamma$  transitions leading to a continuous distribution of lower energy recoils are more probable. It should be long-lived compared to the detector response time. We thus define a figure of merit (FoM) of a target nucleus as:

$$FoM = \sigma_{n,\gamma} \times Y_{ab} \times I_\gamma^s. \quad (1)$$

Table I shows these quantities for W and Ge, which are of interest for a number of ongoing and future experiments [9, 18–21] using  $\text{CaWO}_4$ ,  $\text{PbWO}_4$  or Ge detectors. To obtain the single  $\gamma$  calibration lines and the continuous recoil distributions from the multi- $\gamma$  cascades we employ the simulation software FIFRELIN developed at CEA (France). This code has been validated in different physics cases, from the description of fission fragments [25] to the validation of n-Gd cascades in neutrino detection [26]. Good agreement has also been obtained with independent calculations performed with the DICEBOX code [27]. After thermal neutron capture (s-wave), the nucleus is in an excited state ( $E \simeq S_n, J, \pi$ )<sub>exc</sub> deduced from reaction selection rules. Single- $\gamma$  transition

Table I. Nuclear data for W and Ge isotopes. Quantities in columns 4 to 6 refer to the compound nuclei following neutron capture (See text for notation).

Target Isotope	$Y_{ab}$ [22] (%)	$\sigma_{n-\gamma}$ [23] (barn)	$S_n$ [24] (keV)	$I_\gamma^s$ [24] (%)	Recoil (eV)	FoM
$^{182}\text{W}$	26.50	20.32	6191	13.94	112.5	7506
$^{183}\text{W}$	14.31	9.87	7411	5.83	160.3	823
$^{184}\text{W}$	30.64	1.63	5754	1.48	96.1	74
$^{186}\text{W}$	28.43	37.89	5467	0.26	85.8	281
$^{70}\text{Ge}$	20.52	3.05	7416	1.95	416.2	122
$^{73}\text{Ge}$	7.76	14.70	10196	0.0	754.9	-
$^{74}\text{Ge}$	36.52	0.52	6506	2.83	303.2	54

is favored when the primary excited state and ground-state quantum numbers allow multipolarity  $L=1$  transitions. To build the level scheme of a nucleus FIFRELIN first includes all available experimental data (energy levels, branching ratios) from the RIPL-3 [28], ENSDF [29] or EGAF [24] databases. Since the complete level scheme is not experimentally known, it is completed by sampling levels in the nuclear level density Composite Gilbert-Cameron Model [28]. The transition probabilities between levels are computed from the EGLO radiative strength function [28] for E1 transitions, SLO for other multipolarities. The conversion electrons are given by the BrIcc coefficients [30]. A transition between two levels is sampled among all possible transitions, fully characterizing the emitted particles ( $E, J, \pi$ ). This is repeated until the ground state is reached. Thus by construction all  $\gamma$ -cascades have the correct total energy. More details on the algorithm can be found in [31].

As an example, the predicted gamma and conversion electron spectra emitted by an individual atom of  $^{183}\text{W}$  are shown in Fig. 1. This isotope is of particular interest because it arises from a neutron capture on  $^{182}\text{W}$ , which as seen in Table I, will be the most important neutron capturing nuclide in  $\text{CaWO}_4$ . The two  $\gamma$ -lines of highest energy, at 6.190 and 6.144 MeV, are intense and well separated from the rest of the spectrum, favoring a strong calibration signal. The nuclear recoils from these two photons,  $E_\gamma^2/2M$ , are too close to be resolved by the detector but the resulting mean energy is well known from the relative branching ratios of both lines measured at the sub-% level [24]. We note that while uncertainties in  $I_\gamma^s$  may affect the expected signal-to-background ratio, it does not affect the position of the calibration peaks.

The lower energy  $\gamma$ 's emitted in the nuclear cascade have a short attenuation length, a high conversion coefficient, and will have a high probability of interacting in a cm-dimension crystal. However, due to the nature of electromagnetic interactions and the initial energy always large (at least several keV) with respect to the 100 eV-range, the deposited energy will very rarely be in the region-of-interest (ROI). The exception can be electron events very close to the surface of the crystal where most

of the energy escapes or very forward Compton scattering of photons. But the total phase-space of these events is very small and the ROI is populated by virtually pure nuclear recoils, induced by single and multi- $\gamma$  cascades with no conversion electrons and  $\gamma$ -ray(s) escaping the detector without interaction.

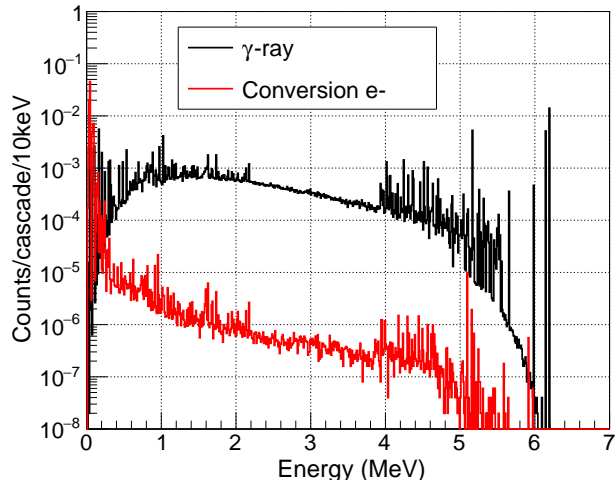


Figure 1. Gamma (black) and conversion electron (red) spectra from the de-excitation of an individual  $^{183}\text{W}$  atom following a neutron capture on  $^{182}\text{W}$ , as predicted by the FIFRELIN code with experimental levels taken from the RIPL-3 and EGAF databases.

Two experimental variants of this method are possible. In the first, the emitted gamma(s) are detected, giving an additional signal in coincidence with that in the detector. Or, it may be that the background reduction and the energy resolution of the detector are sufficient in themselves to reveal the peak in the energy spectrum which corresponds to the sought-for nuclear recoil. Somewhat surprisingly, we find in the explicit experimental configuration described below, that this second, simpler, variant is possible with  $\text{CaWO}_4$  crystals. That is, the nuclear recoils can be seen, even without  $\gamma$ -tagging. This experiment, in addition to establishing the principle, will allow a direct calibration of the NUCLEUS detectors with nuclear recoils at energies of interest for CEvNS [32].

The experiment we now consider in detail comprises a cryogenic  $\text{CaWO}_4$  detector with a thermal neutron beam from a reactor. The  $\text{CaWO}_4$  crystal is cubic, of length 5 mm on a side, and has achieved energy thresholds of  $\sim 20$  eV along with an energy resolution of 3.4 eV [7, 33], safely taken as 5 eV in the following simulations. We first consider the permissible intensity of the neutron beam. The relatively long pulse decay times, of the order of 10 ms, imply stringent rate constraints on cryogenic detectors. A dedicated measurement to determine the optimal event rate was performed by injecting artificial heater

pulses corresponding to the relevant energies at various rates. An optimal event rate of 20 Hz was found for a gram-scale detector, corresponding to an effective rate of  $\sim 10$  Hz after cuts. Here the energy deposits from the conversion electrons and low energy  $\gamma$ -rays, although they do not significantly enter into the ROI, play an important role, since the induced pulses have a large amplitude with a long recovery time.

The thermal neutron beam and the transport of all emitted photons and electrons from neutron-capture vertices were studied with version 10.04.p02 of GEANT4 [34]. The neutron\_HP package based on ENDF/B-VII.1 evaluated nuclear data [35] and the NCRYSTAL library [36] were used to describe the neutron-crystal interactions. The EMZ physics list allows a record of all energy deposits induced in the detector, down to the few eV scale.

We find that an incident thermal neutron flux of  $400 \text{ n/cm}^2/\text{s}$  fulfills the rate specification with an associated n-capture rate in the  $\text{CaWO}_4$  crystal of 9.9 Hz and with a rate of 0.25 Hz for the sought-for signal from the single- $\gamma$  transitions (Table II).

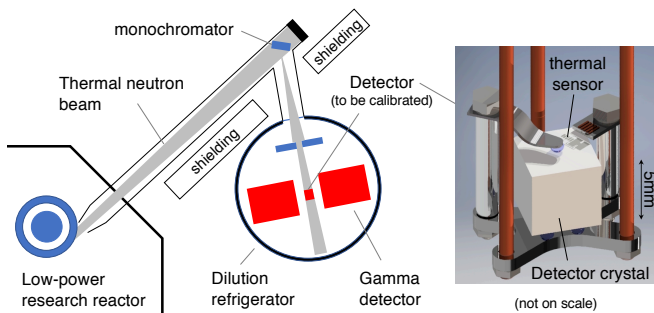


Figure 2. Illustration of the experimental concept using a low-power TRIGA reactor to produce a low intensity, directional and purely thermalized neutron beam. The configuration of the beam line tangential to the core strongly reduces the gamma and fast neutron backgrounds. Inset: example detector assembly in the cryostat with thermal sensor and low mass holder to reduce n-induced backgrounds. Sizes of the refrigerator and the detector assemblies are magnified for clarity.

A high-quality neutron beam with low background despite this very low flux could be available at a low power reactor such as the 250 kW TRIGA-Mark II reactor operating in Vienna [37]. Beamlines at this facility deliver a thermal neutron flux of  $10^4 \text{ n/cm}^2/\text{s}$ . Bragg diffraction from a monochromator crystal inserted into the beamline, in combination with corresponding beam optics, can provide a collimated thermal neutron beam of the desired flux, with no need for further flux attenuation. Flux values of a few  $100 \text{ n/cm}^2/\text{s}$  are typical for experiments with monochromatic neutrons at the Vienna TRIGA reactor, see e.g. [38, 39]. The fast neutron component, that could

Table II. Rates in a  $5 \times 5 \times 5 \text{ mm}^3$   $\text{CaWO}_4$  crystal in an incident flux of  $400 \text{ neutron/cm}^2/\text{s}$ . When the simulation produces no events, the upper limit is set from the statistical accuracy.

	Total ( $s^{-1}$ )	ROI ( $s^{-1}$ )
	$E > 20 \text{ eV}$	$20 < E < 200 \text{ eV}$
<b>Background:</b>		
1) Multi- $\gamma$ 's	9.65	2.15
2) Reactor OFF	0.16	0.08
3) Reactor ON		
$\gamma$ 's	0.05	$< 3 \times 10^{-3}$
neutron beam	0.046	$< 5 \times 10^{-6}$
<b>Signal:</b>	0.25	0.25

induce nuclear recoils in the ROI *via* elastic scattering, is highly suppressed in the extraction of thermal neutrons from the reactor pool and then by the Bragg diffraction in the monochromator. The layout of the neutron beamline and the cryostat proposed here is shown in Fig. 2.

Concerning backgrounds, the high energy resolution of the detector is critical in keeping the mono-energetic calibration events in a small energy band, helping to suppress the more spread-out background. For the present purposes we define a region of interest  $20 < E < 200 \text{ eV}$  for the energy deposit in the crystal. This region encompasses the single- $\gamma$  recoils expected for W isotopes (Table I). Backgrounds will be processes which give energy deposits in the ROI other than those from the nuclear recoils induced by the single- $\gamma$  transitions. These backgrounds will include: 1) Neutron-capture induced multi- $\gamma$  cascades which give energy deposits in the ROI; 2) 'Reactor-off' backgrounds, ambient and cosmogenic activity from the detector apparatus and cosmic rays; 3) Reactor induced backgrounds from the neutron beam or other sources.

Our conclusion is that 1) is the dominant background. To explain this, we first note that the multi- $\gamma$  transition is the most probable process following neutron capture. From detailed GEANT4 simulations we found that 21.5% of the neutron-captures (2.15 Hz in our study) lead to multi- $\gamma$  cascades with no energy deposit from the photons or electrons but with a nuclear recoil in the ROI. Concerning 2) the 'reactor-off' background was measured at the earth's surface, with no specific shielding around the cryostat at the level of  $\sim 10 \text{ events/day/eV}$  for a NUCLEUS crystal [7, 33]. This data is taken as a safe estimate for this study but it can of course be measured at the real site when the reactor is off. The situation for 3), the reactor-related background, is more complicated. First there are the backgrounds induced by the neutron beam itself. Dedicated GEANT4 simulations, including the crystal holder illustrated in Fig. 2 show that a simple configuration of boron-loaded screens used to collimate the beam upstream of the crystal and to stop it downstream of the crystal efficiently suppresses this background. Then, measurements of the ambient

neutron and  $\gamma$  spectra have been performed in the experimental hall of the TRIGA reactor. They are taken as references for absolute normalization and estimation in simulations for the detector rate. The low ambient flux of thermal neutrons can be suppressed by a thin layer of borated shielding. A complementary GEANT4 simulation implementing a biased transport of the neutrons from the core shows that the residual flux of fission fast neutrons is fully negligible at the exit of the reactor pool.

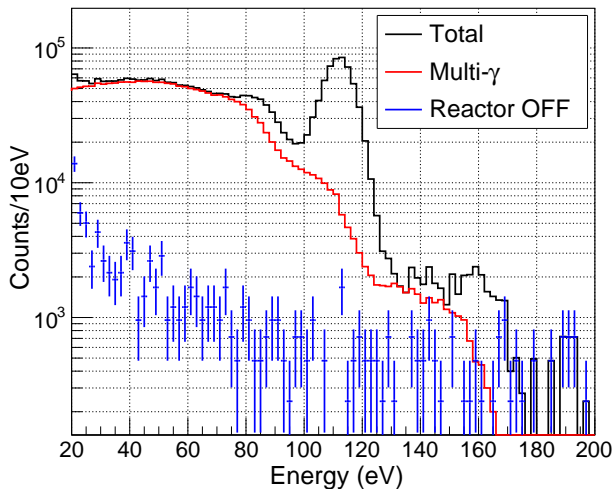


Figure 3. Simulated response of a 0.76 g  $\text{CaWO}_4$  detector with 5 eV energy resolution, exposed to a flux of  $400 \text{ n/cm}^2/\text{s}$  during 2.9 days. The red and blue spectra correspond to the main background contributions labelled 1) and 2) in Table II respectively. One notes that in the total spectrum (black) the calibration peak at 112 eV is clearly visible above background.

All contributions to signal and background are summarized in Table II. The expected spectra of energy deposits in the ROI are shown in Fig. 3 for a run time of 2.9 days, with a NUCLEUS  $\text{CaWO}_4$  crystal. The neutron captures on all elements are simulated but calcium and oxygen have a negligible contribution (97.6% of the n-captures in  $\text{CaWO}_4$  involve tungsten). The red line is for the dominant multi- $\gamma$  background (1), the blue points are from the surface measurement, corresponding to background (2), and finally the black line shows the total, including the sought-for signal from single- $\gamma$ 's.

The peak corresponding to the single- $\gamma$  transitions of  $^{183}\text{W}$  is clearly visible at 112 eV, with a signal-to-background ratio around 10. This makes this calibration method very robust for the  $\text{CaWO}_4$  case. The mean position of this peak could be determined with 1% accuracy in less than one hour of data taking. Two other calibration peaks are visible at 86 eV and 160 eV corresponding to the  $^{187}\text{W}$  and  $^{184}\text{W}$  isotopes respectively. However their signal-to-background is significantly lower and the measurement of the position of these peaks be-

come very sensitive to the uncertainties of the reactor off background and the simulated multi- $\gamma$  decay schemes.

Thus we investigated the other experimental variant, namely detection of the primary  $\gamma$  in coincidence with the signal in the detector. Two cylindrical BGO crystals ( $\varnothing 3'' \times 3''$ ) placed on both sides of the detector at 4 cm distance from its surface (Fig. 2) were considered as an example of a good compromise between rate, energy resolution, detection efficiency, compactness and timing of the light signal detected by a bolometric photodetector. The assumed performances were taken from measurements with a  $\varnothing 20 \times 20 \text{ mm}^3$  BGO detector (described e.g. in [40]) operated at 20 mK at the IJCLab (Orsay, France). In particular a 5.2% energy resolution (FWHM) was obtained for the  $^{208}\text{Tl}$  line at 2.615 MeV. We find that requesting a  $\gamma$  to be detected in one of the two BGO crystals with an energy selection centered on the energy of a single- $\gamma$  transition and a width of  $\pm 0.2 \text{ MeV}$  ( $\simeq 2 \sigma$  of energy resolution) will allow a %-level determination for the 86 eV and 160 eV peaks for tungsten, with reduced effects from the multi- $\gamma$  induced recoils. Such a measurement would extend the energy range for a  $\text{CaWO}_4$  calibration, improving the study of the detector linearity.

Germanium is of particular interest due to its widespread use for the detection of low energy recoils [8, 10, 11, 41, 42]. We have simulated the recoil spectrum in a Ge detector, considering the main capture isotopes listed in Table I and assuming energy, time responses and 'reactor off' background as measured by the EDELWEISS collaboration [10]. The  $^{74}\text{Ge}$  calibration peak, expected at 754 eV, is unfortunately suppressed because of the large multipolarity of the  $S_n$  to ground-state transitions. The other peak expected at 416 eV from the single- $\gamma$  of  $^{74}\text{Ge}$  is overwhelmed by the large and steep multi- $\gamma$  background due to the finite resolution of the detector ( $\sigma=20 \text{ eV}$ ) [10]. Figure 4 illustrates how a coincidence with the high energy  $\gamma$ -ray will allow recovery of the calibration peak. The cut for the photon is centered on 7416 keV, the nominal energy of the single- $\gamma$  transition, with the same  $\pm 200 \text{ keV}$  width. This coincidence not only suppresses the multi- $\gamma$  background but also makes its distribution a lot more symmetrical around the peak position. Therefore only a modest knowledge of the residual background is needed for fitting. A simple fit with two Gaussians, one for the calibration peak and the other for the background, recovers the correct calibration energy to better than 1%. A second calibration line is expected at 303 eV from Table I but with lower intensity. It is barely visible in the top plot of Figure 4 and difficult to isolate even with  $\gamma$ -tagging.

This work suggests a number of interesting issues for further study, as well as many applications. We will examine other detector materials and study the compromise between better rejection of the multi- $\gamma$  cascades but degraded resolution when increasing the detector size. Here we have studied the situation for complex nuclei,

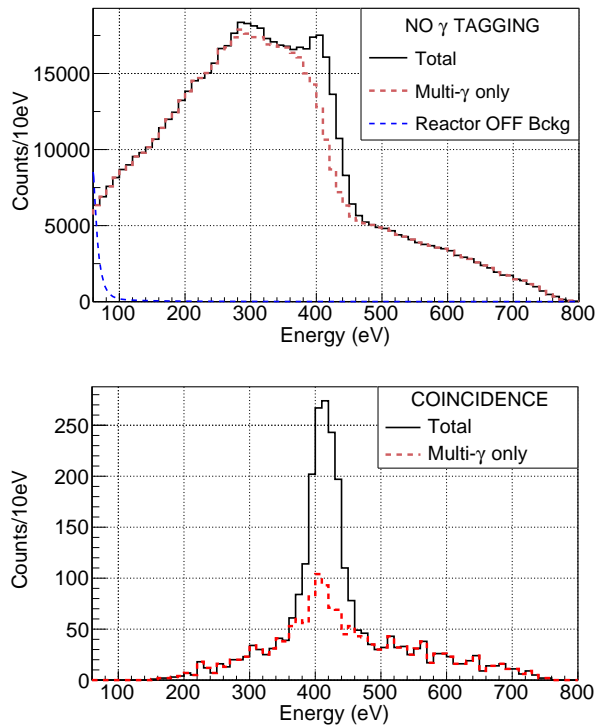


Figure 4. Top: simulated spectrum of nuclear recoils in a 33 g Ge detector assuming an incident flux of 5 n/cm<sup>2</sup>/s (corresponding to about 2 n-capture/s) for 7 days and a 20 eV energy resolution. Bottom: spectrum obtained from the same simulation when requiring a reconstructed energy in the [7.2–7.6] MeV range in one of the two  $\varnothing 3'' \times 3''$  cylindrical BGO  $\gamma$ -detectors operated inside the cryostat.

as relevant to a number of current projects such as NUCLEUS. For the lighter nuclei there is also an interesting but somewhat different situation which is studied in a parallel paper [43]. The arrangement with two  $\gamma$  detectors could be used to select "back-to-back" configurations. Such triple coincidences between the central detector and two  $\gamma$ -rays would select events in the continuous spectrum of lower energy recoils, offering an extended energy range for calibration. The neutron capture technique could considerably reduce the uncertainties in the low-energy ionization quenching factor of Ge detectors [44] currently limiting their sensitivity. The combination of these measurements with novel electron-recoil techniques will allow one to acquire a thorough knowledge of the relevant phonon and ionization processes at low energies. Finally this technique could also be used to study and validate directional sensitivity in cryogenic detectors [45].

- \* david.lhuillier@cea.fr
- [1] D. B. Kaplan, Phys. Rev. Lett. **68**, 741 (1992).
  - [2] J. L. Feng and J. Kumar, Phys. Rev. Lett. **101**, 231301 (2008), arXiv:0803.4196 [hep-ph].
  - [3] R. Essig, A. Manalaysay, J. Mardon, P. Sorensen, and T. Volansky, Phys. Rev. Lett. **109**, 021301 (2012), arXiv:1206.2644 [astro-ph.CO].
  - [4] T. Lin, H.-B. Yu, and K. M. Zurek, Phys. Rev. D **85**, 063503 (2012).
  - [5] D. Z. Freedman, D. N. Schramm, and D. L. Tubbs, Ann. Rev. Nucl. Part. Sci. **27**, 167 (1977).
  - [6] A. Drukier and L. Stodolsky, Phys. Rev. D **30**, 2295 (1984).
  - [7] R. Strauss et al., Phys. Rev. D **96**, 022009 (2017), arXiv:1704.04317 [physics.ins-det].
  - [8] R. Agnese et al. (SuperCDMS), Phys. Rev. D **97**, 022002 (2018), arXiv:1707.01632 [astro-ph.CO].
  - [9] A. H. Abdelhameed et al. (CRESST), Phys. Rev. D **100**, 102002 (2019), arXiv:1904.00498 [astro-ph.CO].
  - [10] E. Armengaud et al. (EDELWEISS), Phys. Rev. D **99**, 082003 (2019), arXiv:1901.03588 [astro-ph.GA].
  - [11] Q. Arnaud et al. (EDELWEISS), Phys. Rev. Lett. **125**, 141301 (2020), arXiv:2003.01046 [astro-ph.GA].
  - [12] A. Manalaysay et al., Rev. Sci. Instrum. **81**, 073303 (2010), arXiv:0908.0616 [astro-ph.IM].
  - [13] T. H. Joshi, S. Sangiorgio, A. Bernstein, M. Foxe, C. Haggmann, I. Jovanovic, K. Kazkaz, V. Mozin, E. B. Norman, S. V. Pereverzev, F. Rebassoo, and P. Sorensen, Phys. Rev. Lett. **112**, 171303 (2014).
  - [14] J. Lindhard and M. Scharff, Phys. Rev. **124**, 128 (1961).
  - [15] S. Ovchinnikov, G. Ogurtsov, J. Macek, and Y. Gordeev, Physics Reports **389**, 119 (2004).
  - [16] J. B. Birks, Proceedings of the Physical Society. Section A **64**, 874 (1951).
  - [17] L. Stodolsky, Phys. Today **44N8** (1991).
  - [18] R. Strauss et al., Eur. Phys. J. C **77**, 506 (2017), arXiv:1704.04320 [physics.ins-det].
  - [19] J. Billard et al., J. Phys. G **44**, 105101 (2017), arXiv:1612.09035 [physics.ins-det].
  - [20] G. Agnolet et al. (MINER), Nucl. Instrum. Meth. A **853**, 53 (2017), arXiv:1609.02066 [physics.ins-det].
  - [21] L. Pattavina, N. Ferreiro Iachellini, and I. Tamborra, Phys. Rev. D **102**, 063001 (2020), arXiv:2004.06936 [astro-ph.HE].
  - [22] J. Meija, T. B. Coplen, M. Berglund, W. A. Brand, P. D. Bièvre, M. Gröning, N. E. Holden, J. Irrgeher, R. D. Loss, T. Walczyk, and T. Prohaska, Pure and Applied Chemistry **88**, 293 (01 Mar. 2016).
  - [23] D. A. Brown et al., Nuclear Data Sheets **148**, 1 (2018).
  - [24] R. B. Firestone et al., Nucl. Data Sheets **119**, 79 (2014).
  - [25] O. Litaize et al., Eur. Phys. J. A **51**, 1 (2015).
  - [26] H. Almazán et al., Eur. Phys. J. A **55**, 183 (2019).
  - [27] F. Bečvář, Nucl. Instr. Meth. Phys. Res. A **417(2-3)**, 434 (1998).
  - [28] R. Capote et al., Nucl. Data Sheets **110**, 3107 (2009).
  - [29] From ENSDF database as of March, 2020. Version available at <http://www.nndc.bnl.gov/ensarchivals/> (2020).
  - [30] T. Kibédi et al., Nucl. Instr. Meth. Phys. Res. A **58**, 202–228 (2008).
  - [31] D. Regnier et al., Comput. Phys. Commun. **51**, 19 (2016).

- [32] G. Angloher et al. (NUCLEUS), *Eur. Phys. J. C* **79**, 1018 (2019), arXiv:1905.10258 [physics.ins-det].
- [33] G. Angloher et al. (CRESST), *Eur. Phys. J. C* **77**, 637 (2017), arXiv:1707.06749 [astro-ph.CO].
- [34] J. Allison et al., *Nucl. Instr. Meth. Phys. Res. A* **835**, 186 (2019).
- [35] D. A. Brown et al., *Nuclear Data Sheets* **107**, 2931–3060 (2006).
- [36] X.-X. Cai and T. Kittelmann, *Comput. Phys. Commun.* **246**, 106851 (2020).
- [37] History, Development and Future of TRIGA Research Reactors, Technical Reports Series No. 482 (INTERNATIONAL ATOMIC ENERGY AGENCY, Vienna, 2016).
- [38] J. Erhart et al., *Nat. Phys.* **8**, 185 (2012).
- [39] E. Jericha et al., *J. Appl. Crystallogr.* **36**, 778 (2003).
- [40] P. de Marcillac, N. Coron, G. Dambier, J. Leblanc, and J.-P. Moalic, *Nature* **422**, 876 (2003).
- [41] J. Hakenmüller et al., *Eur. Phys. J. C* **79**, 699 (2019), arXiv:1903.09269 [physics.ins-det].
- [42] C. Aalseth et al. (CoGeNT), *Phys. Rev. D* **88**, 012002 (2013), arXiv:1208.5737 [astro-ph.CO].
- [43] L. Stodolsky, to be published.
- [44] D. Barker and D.-M. Mei, *Astropart. Phys.* **38**, 1 (2012).
- [45] S. Griffin, S. Knapen, T. Lin, and K. M. Zurek, *Phys. Rev. D* **98**, 115034 (2018).